Feasibility Assessments of a Hybrid Turboelectric Medium Altitude Long Endurance Unmanned Aerial Vehicle

Gokcin Cinar*, Alexander A. Markov†, Jonathan C. Gladin‡, Elena Garcia§, and Dimitri N. Mavris¶
Aerospace Systems Design Laboratory, School of Aerospace Engineering,
Georgia Institute of Technology, Atlanta, Georgia 30332

Soumya S. Patnaik‖
Aerospace Systems Directorate, Air Force Research Laboratory, Dayton, Ohio 45433

Electrified propulsion systems can provide potential environmental and performance benefits for future aircraft. The choice of the right propulsion architecture and the power management strategy depends on a number of factors, the airframe, electrification objectives and metrics of interest being the most critical ones. Therefore, the generic advantages and disadvantages of various electrified propulsion architectures must be quantified to assess feasibility and any possible benefits. Moreover, the objectives and the metrics of interest can be different for military applications than commercial ones. This research investigates the feasibility of turboelectric and hybrid turboelectric propulsion architectures integrated within a medium altitude long endurance surveillance unmanned aerial vehicle. The electrified propulsion system is desired to provide the same endurance and takeoff and landing field length characteristics of the baseline aircraft. This paper presents the results of the first phase of this research where only the electrified propulsion system is sized while the airframe is kept fixed. Physics-based models and a generic mission analysis methodology are used to evaluate the performance of the major subsystems of the propulsion system and to provide a full flight mission history. A state of the art rechargeable battery is employed for the hybrid case. Various power management strategies where the battery is discharged and charged in different flight segments are explored for varying sizes of battery packs. Results indicate that, while none of the architectures can offset the added weight and the efficiency factors of the electrical components as expected, the hybrid turboelectric propulsion architecture can provide fuel burn and performance benefits when sized for, and operated under, a specific set of power management strategies.

I. Introduction

Electrified aircraft propulsion (EAP) technologies can reduce fuel burn and harmful aircraft emissions, mitigate noise and lower the maintenance and operating costs. While EAP applications on commercial aircraft are mainly motivated by these objectives, EAP technologies can also be beneficial for military applications by providing an additional source of energy and power thereby improving the aircraft mission and point performance.

NASA designates the all-electric, turboelectric and hybrid electric propulsion as three major research areas within the aerospropulsion category [1]. Aircraft which solely depend on electric motors and rechargeable batteries cannot achieve the same flight performance as aircraft with conventional propulsion systems, mainly due to the low gravimetric energy density of batteries and thermal challenges. Therefore, partially electrified propulsion systems, i.e. turboelectric and hybrid electric propulsion systems, are envisioned as a middle step towards electrified propulsion systems.

In turboelectric propulsion system architecture, the mechanical energy at the output of the fuel burning engine is first converted into electricity by the generator. This electrical energy is used to drive the electric motor which in return generates shaft power to drive the fan(s) or propeller(s). This electrical energy can be used to charge the battery and/or to generate shaft power by the electric motor. If there exists a second type of energy source, such as a rechargeable

*Research Engineer II, ASDL, School of Aerospace Engineering, Georgia Tech, AIAA Member
†Graduate Research Assistant, ASDL, School of Aerospace Engineering, Georgia Tech, AIAA Student Member
‡Research Engineer II, ASDL, School of Aerospace Engineering, Georgia Tech, AIAA Member
§Senior Research Engineer, ASDL, School of Aerospace Engineering, Georgia Tech, AIAA Member
¶S.P. Langley Distinguished Regents Professor and Director of ASDL, School of Aerospace Engineering, Georgia Tech, AIAA Fellow
‖Senior Engineer, Aerospace Systems Directorate, Air Force Research Laboratory, AIAA Senior Member

battery, then the propulsion system is called a hybrid turboelectric architecture (also known as series hybrid electric). In this architecture, the electrical energy from the generator can also be used to recharge the battery. A schematic of a hybrid turboelectric propulsion system architecture is given in Figure 1.

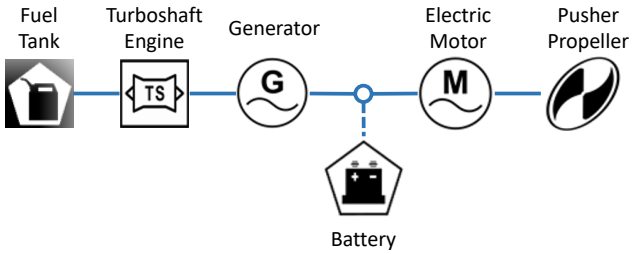

Fig. 1 Schematic of a hybrid turboelectric powertrain.

Although hybrid turboelectric propulsion architectures partially rely on fossil fuel burning engines, they can still provide fuel burn savings and other performance benefits. There are three main sources of potential benefits associated with these architectures: i) decoupling the engine from the main transmission system, ii) energy boost provided by the battery, and iii) powertrain being less complex relative to other hybrid electric configurations.

First, when the engine is decoupled, it can run at its peak efficiency independent of the RPM of the transmission system. The provided flexibility of locating the engine-generator set away from the propeller(s) also enables unconventional airframe-propulsion system integration and configurations, such as seen on the NASA STARC-ABL [2], N3-X [3], and ECO-150 [4] concepts, which can improve aerodynamic efficiency. Second, in contrast to gas turbine and internal combustion engines, electric motors do not lapse with altitude and velocity. A rechargeable battery in a hybrid system can provide the power needed to boost the high-performance flight maneuvers and mission segments such as takeoff and climb. This strategy is called an "e-boost". Third, this architecture does not require a complex power split unit which would add additional weight to the system.

However, the benefits must offset the added weight and the efficiency factors of the electrified powertrain subsystems. There are three propulsion devices in this architecture, namely the engine, generator and electric motor, as shown in Figure 1. All three propulsion devices need to be sized for the maximum sustained power for high performance flight; which brings an increased weight penalty. Although a torque amplification device can be integrated to improve the performance of the motor and hence reduce its size, the motor must still be significantly more powerful than a motor used in a parallel hybrid architecture. [5, 6]

The literature on electrification of larger unmanned aerial vehicles (UAVs) shows that the tradeoff between the aerodynamic and performance improvements, and the added weight and efficiency factors manifests itself differently in different classes and configurations of vehicles. The overall objective for electrification, such as technology demonstration, emission and noise mitigation, performance improvements, etc., also drives the architecture selection. These considerations lead to the selection of diverse propulsion system architectures. Some examples of electrification of middle-to-large size of UAVs are given here.

Litherland et al. [7] examined the feasibility of using solid-oxide fuel cells as a secondary energy source in a hybrid electric architecture on a Class IV UAV. Finger et al. [8] compares hybrid electric propulsion systems on a range of aircraft sizes, namely general aviation aircraft, transport aircraft, a medium altitude long endurance (MALE) UAV, and vertical takeoff and landing air taxi. In this research, a parallel hybrid electric propulsion architecture with an internal combustion engine was chosen to investigate and compare the benefits of hybrid, fully electric and fully conventional power management strategies. Fioriti et al. [9] compares a parallel and a series hybrid electric architecture on a MALE UAV and deems that the architectures and the operation modes studied may lead to a reduction in vehicle takeoff gross weight and an increase in safety at the cost of reduced climb performance. A previous study by Cinar et al. [10] provides a methodology to size a fully electrified propulsion system and its application on a hybrid electric MALE UAV.

Based on the literature, the generic advantages and disadvantages of hybrid propulsion architectures must be quantitatively investigated on a specific baseline aircraft to determine feasibility. Furthermore, different power management strategies must be investigated to achieve the maximum benefits. This paper presents the results of the first phase of fundamental research investigating the feasibility and potential benefits on a MALE UAV. In this architecture, a generator, electric motor and a battery are installed and integrated within a conventional propulsion system on a MALE UAV. The first phase is focused on quantifying the benefits of the energy boost and investigation of different power management strategies throughout different flight phases. The second phase, which will be published at a later date, will

present the results of a hybrid turboelectric distributed propulsion system on the same UAV.

II. Baseline Aircraft Selection

A wide range of UAVs were examined to determine what information is available and to down select the baseline aircraft for this study. In total, fourteen vehicles of varying size, powerplant type, mission, and level of design maturity were assessed with an emphasis on propeller driven vehicles [11–25]. All of the vehicles found are listed in Table 1 and the numbers associate with each vehicle are labeled in Figure 2. It should be noted that not all of the vehicles appear in each plot because not all of the data was available for each vehicle. While that literature review focused on conventional propulsion systems using fuel, two proposed hybrid UAVs were also included. One of these, the Hybrid MALE UAV, only exists on paper but the other, the Yabhon United 40, had two produced units and provided some limited data on the electric motor and power used which motivates further study into the hybridization of unmanned aerial vehicles.

Table 1 Vehicle names and data sources from literature review

Vehicle Number	Vehicle Name	MTOW (lb)	Endurance (hr)	Ceiling (ft)	Source
1	Yabhon United	3307	120	22966	[21, 23]
2	Dominator XP	4211	20	30000	[19]
3	Northrop FireBird	5004	40	30000	[20, 23]
4	CH-5 Rainbow	5997	60	23000	[22, 23]
5	AT200	6800	8	20000	[24]
6	Hybrid MALE UAV	8296	30	46000	[25]
7	Heron TP	10251	30	45000	[16, 23]
8	Aurora Orion	11200	120	30000	[15]
9	MQ-9 Reaper	11700	27	45000	[23]
10	P.1HH HammerHead	13550	16	45000	[14, 23]
11	Mantis MALE UAV	19842	30	55000	[11]
12	Euro MALE RPAS	22000	N/A	45000	[12]
13	Bell V-247	29500	8	25000	[18]
14	RQ-4B Global Hawk	32250	34	60000	[17, 23]

The vehicles from the literature review were compared to identify trends and vehicle classes based on maximum take off weight to help determine the most appropriate size for the baseline vehicle. The goal of these comparisons was to select a vehicle which would benefit most from a hybrid architecture application. First, the engine power was compared to the vehicles' maximum take off weight which is shown in Figure 2a.

The red dotted line shows the maximum take off weight where the transition from internal combustion (IC) engines to turboprop (TP) engines occurs which is around 10,000 lbs. This is a general trend as there is one turboprop aircraft below this value and one internal combustion aircraft above this value. The vehicles are also separated by engine type in terms of the engine power which is expected as turboprop engines typically produce more power and larger vehicles require more power. The take away here is that smaller UAVs, those below 10,000 lbs, require less power and thus use internal combustion engines. Engine weight and engine power-to-weight ratio were also compared to the maximum take off weight to better understand how the power system changes with vehicle size. Engine weight did not provide any clear trends, however the engine power-to-weight ratio, shown in Figure 2b, showed a division between internal combustion engines and turboprop engines. This further supports the previous trends as heavier aircraft tend to have higher power to weight ratios which correspond to turboprop engines. The vehicle corresponding to the point within the red circle was the Yabhon United 40 which lacked data about the size and weight of the electric motor making the power to weight ratio appear higher than it actually is.

The vehicles' payload fraction and missions were compared with a focus on range and type of design mission to see if there is a correlation between maximum take off weight (MTOW). The payload weight was also compared but did not provide any conclusive trends so it was omitted. Figure 2c shows the variation of the maximum take off weight with payload fraction with the different colors representing different types of design missions and the labels representing

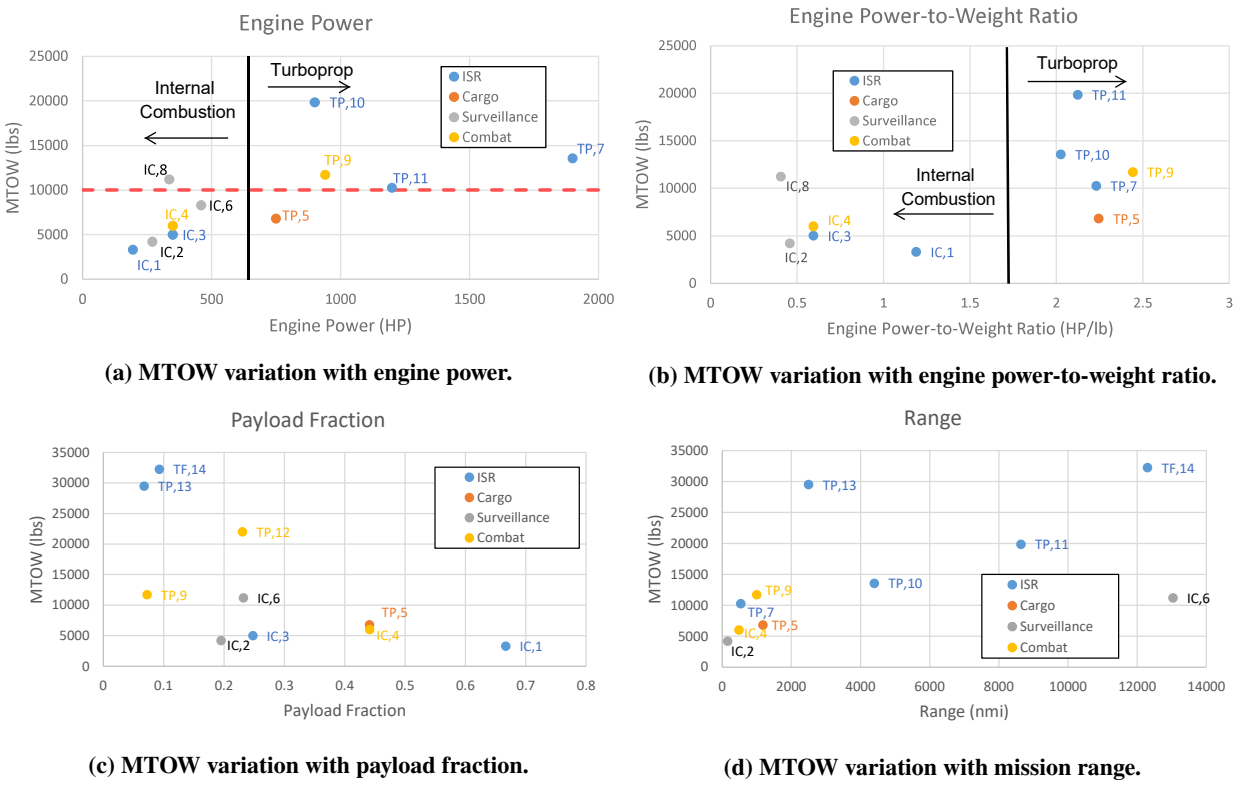

(a) MTOW variation with engine power.

(b) MTOW variation with engine power-to-weight ratio.

(c) MTOW variation with payload fraction.

(d) MTOW variation with mission range.

Fig. 2 Comparisons of vehicles from literature.

the type of engine used. There is no solid distinction between different mission types or types of engine, but there is a diminishing payload fraction trend with increasing maximum take off weight. Based on the vehicles surveyed, the surveillance mission vehicles in Figure 2d are outliers as they are on either extreme of the range spectrum. Another observation from this figure is that the intelligence, surveillance and reconnaissance (ISR) vehicles tend to be the heaviest with maximum take off weights above 12,000 lbs.

A few other comparisons were also performed such as aircraft service ceiling, but the results were trivial and are not included in this paper. After looking at the trends and the possible benefits of adding a hybrid propulsion architecture to the vehicles, the baseline vehicle characteristics were down selected. A vehicle with a turboprop engine was determined to benefit more than one with an internal combustion engine because power could be extracted more efficiently and easily. Electrical components tend to add weight to the vehicle, and because hybrid aircraft are extremely weight sensitive, the vehicle was desired to be as light as possible. The mission type was also considered and based on the literature survey, a combat mission vehicle was of particular interest. A final criteria for down selection was availability of public domain data for the vehicles as a parametric model would need to be created and more data allows for a more accurate model. With these considerations, the MQ-9 Reaper, pictured in Figure 3, was chosen to be the baseline vehicle for this study. Some of the vehicle's specifications are listed in Table 2.

The payload capacity is 850 lbs of internal storage and 3750 lbs of external storage and the endurance can be extended from 27 hours to a maximum of 35 hours. The Reaper also uses a single HoneyWell TPE331-10 engine which can provide up to 1000 horsepower at sea level. The three view of the vehicle with some defined geometry provided values for the vehicle's span, propeller diameter, and length. This three view was also used to determine relative length and sizes of parts of the vehicle which were not explicitly given. Along with the baseline aircraft, a baseline mission was also determined in lieu of one in the public domain. The mission profile is shown in Figure 4 and consists of an idle and take off segment leading to an initial climb and cruise followed by a descent, loiter, and climb section and a return cruise finishing with an initial descent, loiter, final descent, and finally a landing segment.

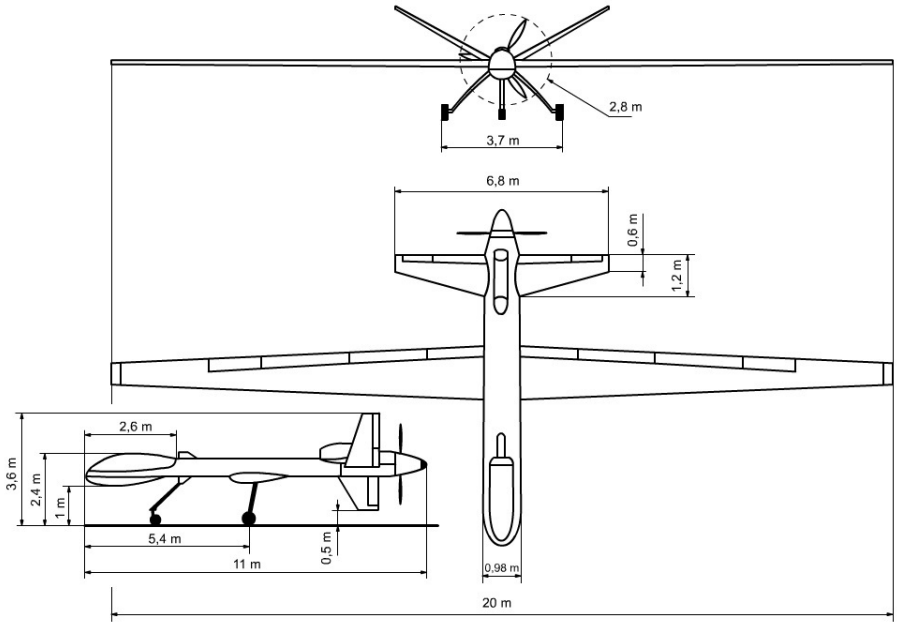

Fig. 3 General Atomics MQ-9 Reaper unmanned aerial vehicle [26].

Table 2 MQ-9 Reaper vehicle and mission specification

Parameter	Value
Mission Type	Combat
MTOW (lbs)	10500
Range (nmi)	1000
Endurance (hr)	27(35*)
Payload (lbs)	850(3750*)
Power Plant	HW TPE331-10
Max Speed (mph)	276

III. Sizing and Synthesis Environment

This study utilizes an in-house sizing and synthesis tool, called “Electrified Propulsion Architecture Sizing and Synthesis”, or E-PASS, which enables design and performance evaluation of any vehicle design, including but not limited to fully and hybrid electric aircraft, and allows for rapid comparisons between diverse propulsion architectures through a novel, matrix-based approach.

The building blocks of E-PASS are shown in Figure 5. E-PASS can be used to size a notional aircraft configuration with a new propulsion architecture (on-design mode) or evaluate the mission performance of an existing concept without sizing it (off-design mode). It has built-in physics-based subsystem models, component-based weight estimation techniques, a power management optimizer and a generic mission analysis module which allows for mission performance evaluations of any propulsion architecture. The interested reader is referred to Ref. [27, 28] for more information on this aircraft design tool.

The technical approach taken in this research utilizes the building blocks 1-to-6 only, as transient analysis of dynamic subsystems is out of the scope of this paper. Furthermore, this is a retrofit study on a notional Reaper UAV with an electrified propulsion architecture and does not involve the re-sizing of the baseline aircraft. Therefore, E-PASS is used in "off-design" mode, i.e. the baseline aircraft size was kept fixed while the electrified propulsion components were sized as described in the upcoming sections.

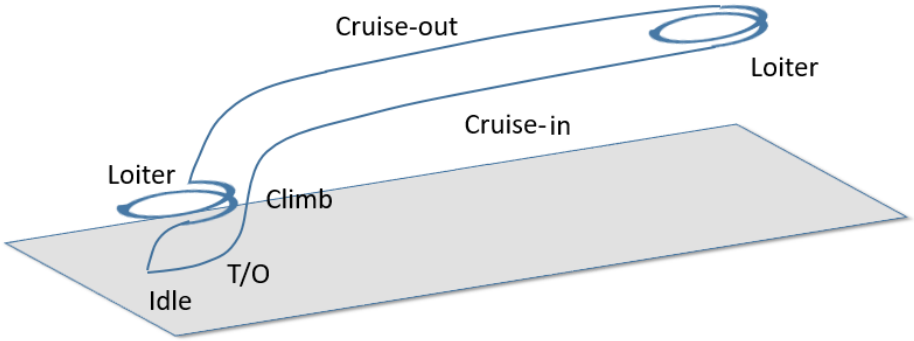

Fig. 4 Baseline mission profile used for analysis of the MQ-9 Reaper.

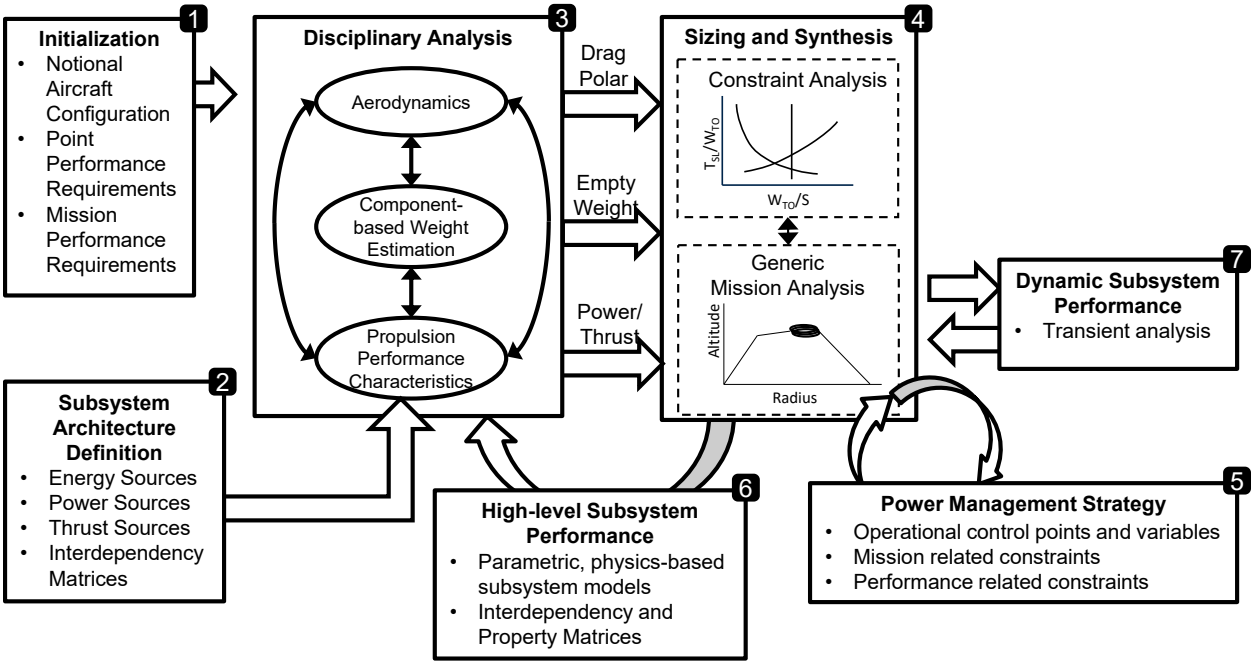

Fig. 5 Building blocks of the electric propulsion architecture sizing and synthesis tool, E-PASS.

IV. Vehicle and Powertrain Modeling

A. Aerodynamics

Due to the lack of public domain aerodynamic data for the Reaper, a quadratic drag polar, represented by Equation 1, was used to model the aerodynamics. The quadratic model consists of two parts, the parasite drag and the lift induced drag, both of which need to be estimated. The parasitic drag coefficient was estimated based on the vehicles skin friction coefficient and wetted area ratio according to Equation 2. Regression plots from Anderson were used for estimating the skin friction coefficient based on Reynolds number and for estimating the wetted area ratio based on wing loading [29]. The skin friction coefficient was validated by a NASA study of a representative Reaper vehicle, the Ikhana research aircraft, which is an early derivative of the MQ-9 Reaper [7].

$$C_D = C_{D_o} + C_{D_i} \tag{1}$$

$$C_{D_o} = C_f \frac{S_{wet}}{S} \tag{2}$$

The lift induced drag is a function of the lift coefficient and the factor k, represented in Equation 3 and Equation 4,

which takes into account the vehicle aspect ratio and the Oswald efficiency factor. The aspect ratio calculation required estimating the wing area based on a three view of the Reaper and the Oswald efficient factor was calculated using a method by Brandt which considers the wing sweep and taper ratio [30]. Excrescence drag was taken to be 20% of the parasite drag according to the methods used in the NASA study. The aerodynamic parameters and the variables used to calculate them are listed in Table 3.

$$C_{D_i} = kC_L^2 \tag{3}$$

$$k = \frac{1}{\pi e AR} \tag{4}$$

Table 3 Aerodynamic parameter values

C_f	W/S	Sweep	Aspect Ratio	$C_{D_{exc}}$	C_{D_o}	S_{wet}/S	e
0.0045	49.5 psf	2.4 deg	18.2	0.2	0.0218	4.0	0.94

B. Propulsion System Modeling and Technology Assumptions

The baseline aircraft employs a Honeywell TPE331-10 turboprop engine driving a pusher propeller at the tail cone through a gearbox with a gear ratio of 20.87 [31]. The baseline propulsion system also includes a small generator. This baseline propulsion system was converted to a turboelectric architecture shown in Figure 1 by removing the gearbox and engine accessories, and adding a generator and an electric motor to the powertrain. The generator and motor were sized to match the same point performance requirements the baseline propulsion system had. Trade studies were performed for a turboelectric propulsion system (without a battery), and a hybrid turboelectric system with varying sizes of battery. The following paragraphs explain how each subsystem of the new powertrain is modeled and sized.

1. Engine

Performance data, as well as dry weight and a breakdown of accessory components, for the TPE331-10 turboprop engine was available from Honeywell [31]. The performance data provided shaft horsepower and fuel flow variation of the engine for a range of airspeeds and altitude, but it needed to be digitized in order to use the data. Figure 6 shows the figure of the data provided as well as the digitized shaft horsepower which corresponds to the grey lines on the figure on the right. The fuel flow data was digitized in the same way but is not shown here. An important note here is that these values of shaft horsepower are the maximum value at a given altitude and airspeed so no part power performance is given. To estimate the part power performance, another turboprop engine of similar size, the PW127M, was used to create normalized part power curves as there was a detailed model of this engine available in house. The normalized curves create a fit to scale the fuel flow for different altitudes and part power settings based on the part power performance of the PW127M engine. To make use of the engine deck within the modeling environment, surrogate models of the shaft horsepower and fuel flow as functions of altitude, Mach number, and part power setting (throttle) were created using MATLAB's neural net toolbox. Additionally, engine accessory component weights were provided and are summarized in Table 4. These weights are significant because they can be removed with the addition of an electric powertrain. For example, a starter battery would no longer be necessary if a battery is present and a gearbox would not be needed because the engine and propeller would be decoupled.

2. Propeller

The propeller deck was generated using the Hamilton Standard Propeller Maps, which plot efficiency contours as functions of advanced ratio, J, and power coefficient, C_p. Each map represents a different propeller designated by three different parameters: Number of blades, activity factor, and design lift coefficient and an example is shown in Figure 7. An equation is provided for the activity factor but it requires knowledge of the blade shape over its span and this information is not available for the baseline vehicle. Similarly, the design lift coefficient of the propeller blade is unknown so choosing the correct map to use is not straight forward, however the advance ratio and power coefficients can be calculated at any point in the mission and an efficiency can be determined for each map. Because the majority of the mission is flown during cruise segments, the cruise conditions were used to calculate the advance ratio and

Table 4 Weights of the accessory components of the TPE331-10 turboshaft engine.

Component	Weight [lbs]
Engine Battery	20
Gearbox	100
Starter Motor	45
Accessories	15
Total	180

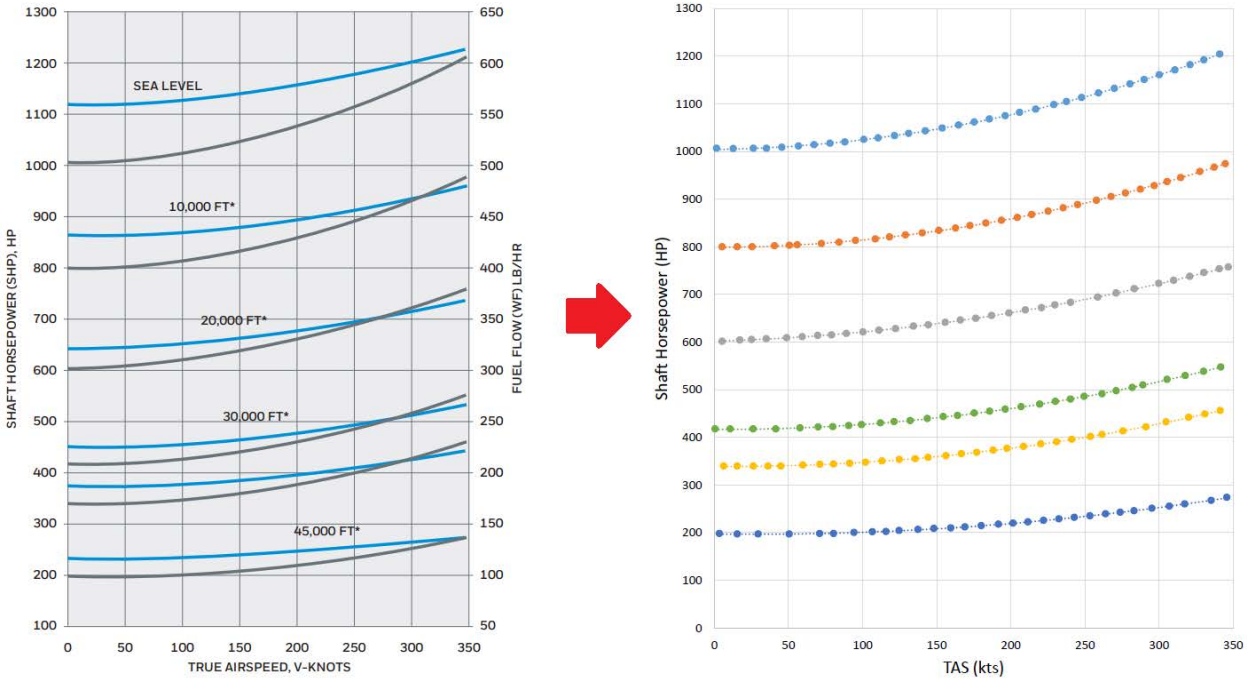

Fig. 6 Engine deck provided by Honeywell for the TPE331-10 Turboprop engine.

power coefficient. The technology level for this study is assumed to be state-of-the-art and some freedom is allowed with respect to the propeller design. Therefore, it is a reasonable assumption to select the map which corresponds to the highest propeller efficiency for the cruise flight conditions. Tabular data of the efficiency maps is available for four-bladed propellers across a wide variety of activity factors and design lift coefficients and this data was used to create a propeller deck.

During cruise, the advance ratio and power coefficient are 0.982 and 0.120 respectively and these values were used to choose the appropriate map. Based on maximum efficiency, the map chosen corresponded to an activity factor of 180 and a design lift coefficient of 0.15, resulting in a propeller efficiency of 0.87. Surrogate models were utilized to streamline this process so that the efficiency at a point in the mission can be calculated using the tabulated data for the chosen map and the flight conditions at that point in time. These models are functions of true air speed, thrust coefficient, torque coefficient, advance ratio, and RPM, however the propeller is assumed to operate at constant RPM so an RPM of 2300 was chosen based on the engine data from Honeywell. This allows the propeller performance to be calculated at any point in the mission and propagates the efficiency throughout the powertrain.

3. Electric Motor

The electric motor parameters were derived from a brushless electric motor designed by Siemens specifically for use on aircraft. The Siemens motor has a maximum power output of 261 kW and a maximum efficiency of 95%, as well as power to weight ratio of 5.22 kW/kg. The efficiency and power to weight ratio were kept identical to the motor, but the

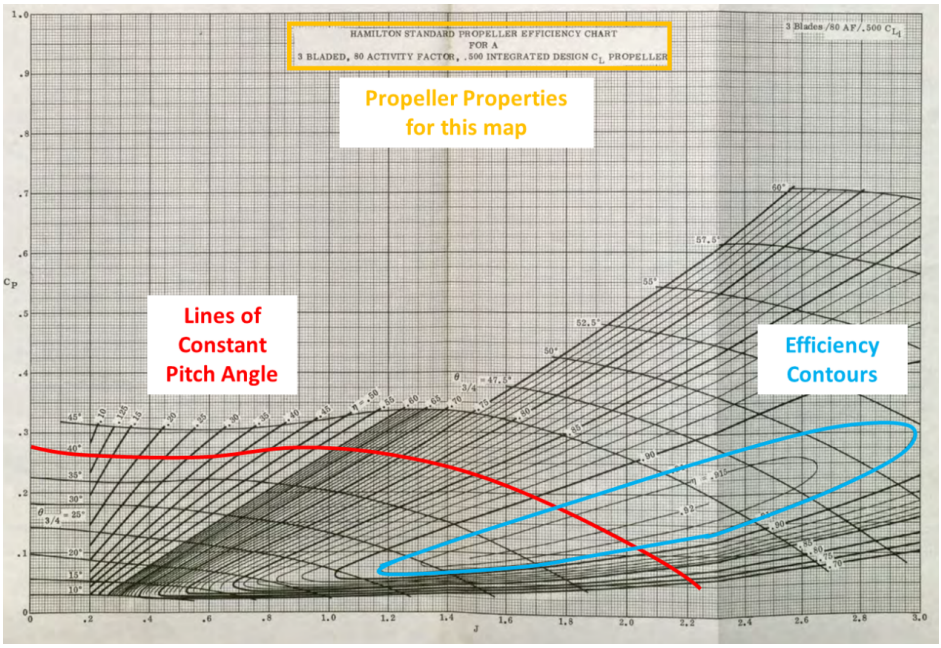

Fig. 7 Example of a Hamilton Standard propeller map [32].

power output was increased to 750 kW to meet the needs of the baseline vehicle. A performance map of the motor was created so that the efficiency could be read at different operating conditions. A rubberized motor Matlab code is used to generate efficiency contours as a function of the motor's speed (RPM) and torque based on the maximum rated power of the motor, the maximum efficiency, and the RPM at maximum efficiency. Figure 8 below shows the contour map for the 750 kW electric motor as well as the efficiency response to changes in torque at an RPM of 2300. The RPM of the motor was chosen to be equal to that of the propeller to avoid gearing. The motor is assumed to operate at a constant RPM during cruise and because cruise segments comprise a majority of the mission, the efficiency is essentially a function of only the torque. On the right side of Figure 8, the red vertical line represents a constant RPM of 2300 with the torque being varied to see how the efficiency responds. The response shows that for a large range of torque above about 750 Nm, the motor efficiency stays above 90%, so the performance is expected to be good within the flight regime of the mission.

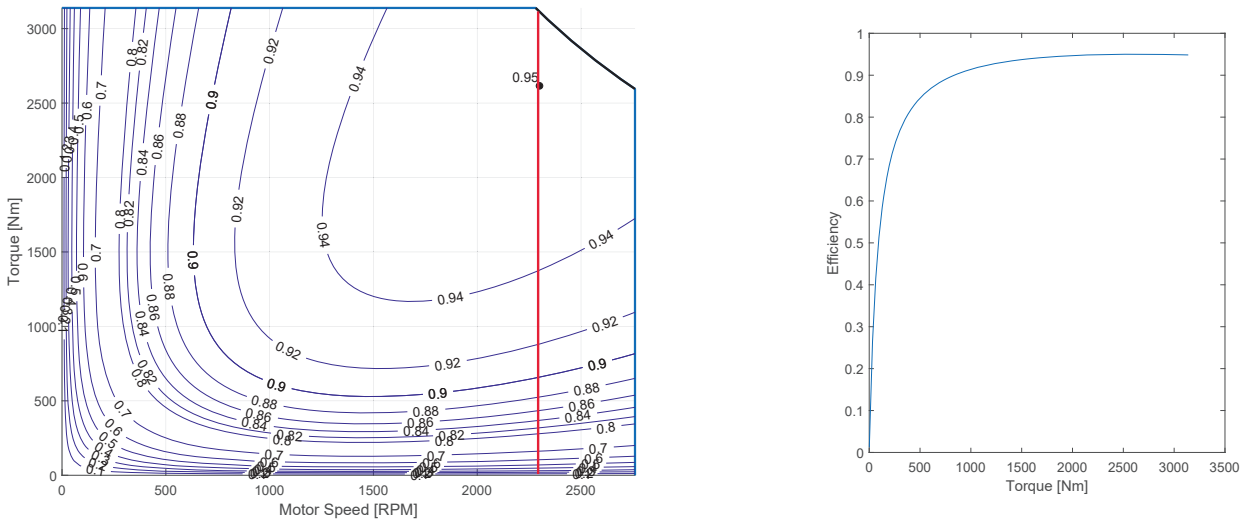

Fig. 8 Performance map of the 750kW motor (left) and efficiency variation with torque (right).

4. Generator

The electric generator parameters were modeled after two Honeywell generators, a 200kW rated power generator and a 1MW rated power generator. To ensure that the generator would be sufficiently large even at maximum engine power at sea level, the rated power of the generator used for the baseline vehicle was chosen to be 750kW. The generator efficiency and power to weight ratio were linearly scaled using the two Honeywell generators. It should be noted that the weights used to calculate power to weight ratios included the generator weight, control unit weight, and rectifier bridge weight. The scaled electric generator had an efficiency of 96% and a power to weight ratio of 5.78 kW/kg with an operating RPM of 19000 which is equal to that of the 1MW generator. A performance map was created for the generator in a similar way to that of the electric motor to be used at different points and conditions during the mission. The map, as well as the variation in efficiency with torque at the operating RPM, is shown in Figure 9 and the same trend is observed.

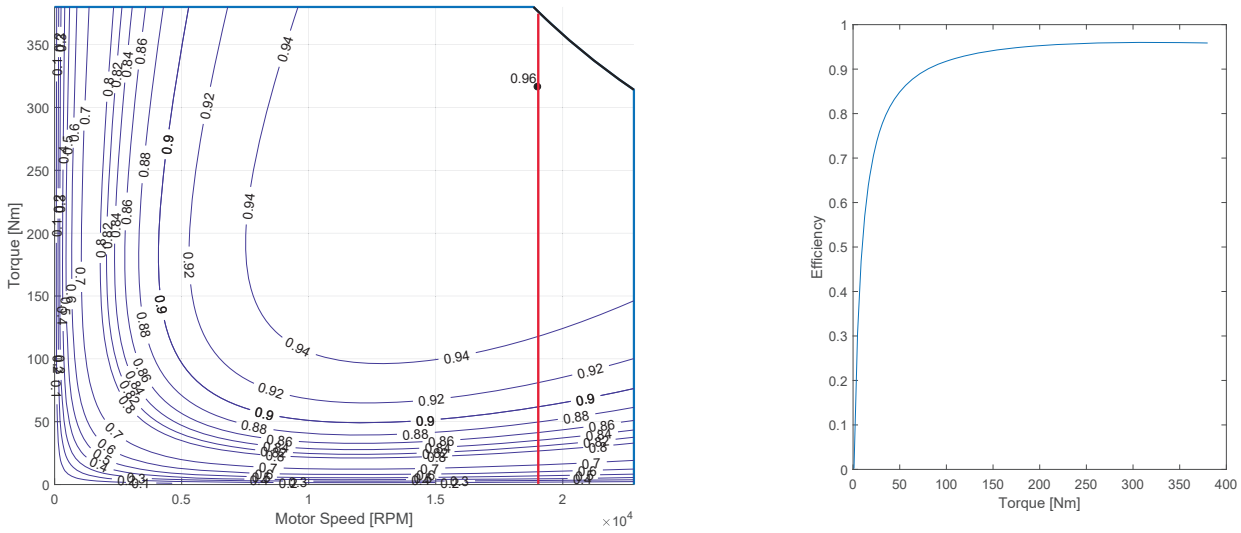

Fig. 9 Performance map of the 750kW generator (left) and efficiency variation with torque (right).

5. Battery

A rechargeable battery was used in hybrid turboelectric architectures. The required battery energy was determined based on the desired hybridization. The battery was sized to provide this required energy such that when fully discharged, it reaches 20% state of charge (SOC) in order not to permanently damage the battery. A specific energy of 200 Wh/kg at the pack level was assumed for the battery technology and is used to determine the battery size. No losses were considered in the battery or during transmission of power from one source to another such as through cables. The maximum take-off weight (MTOW) of the vehicle was to remain constant so addition of the battery and electrical components meant that a trade off was required. Two options were available, one was to keep the payload constant and trade fuel weight for battery and electrical component weight and the other was to trade payload weight instead. The latter was chosen so as to not impact the vehicle's performance and ensure the mission could still be completed as defined.

The required energy to size the battery was determined based on the desired power management schedule. This schedule is an input to the analysis and defines the power flow and splits between the power and energy sources as a function of time. The interested reader can refer to Ref. [28] for a detailed explanations and definitions regarding the power splits between thrust, power and energy sources. In the context of this hybrid turboelectric architecture, power can be split between the energy and power sources in the following scenarios:

i. Generator alone supplies full power to the electric motor (*turboelectric case*)

ii. A combination of generator and battery power drives the electric motor (*hybrid case*)

iii. Battery alone supplies full power to the electric motor (*fully electric case*)

iv. Generator supplies full power to the electric motor and simultaneously charges the battery (*charging case*)

The mission profile can utilize a combination of all four scenarios. The required battery energy is calculated by assuming an initial battery size and running the mission analysis with the desired power management schedule. If the battery is also being charged during flight (i.e. Scenario iv), then the net battery energy (instead of the total required energy) must be calculated to correctly size the battery. If the required energy is greater than the initially assumed energy, then the battery must be upsized. If the available energy is greater than the required energy, then the battery must be downsized to match the final SOC to the minimum SOC limit of 20%. An iteration takes place in this manner until the battery size converges. A flowchart of this battery sizing logic is depicted in Figure 10.

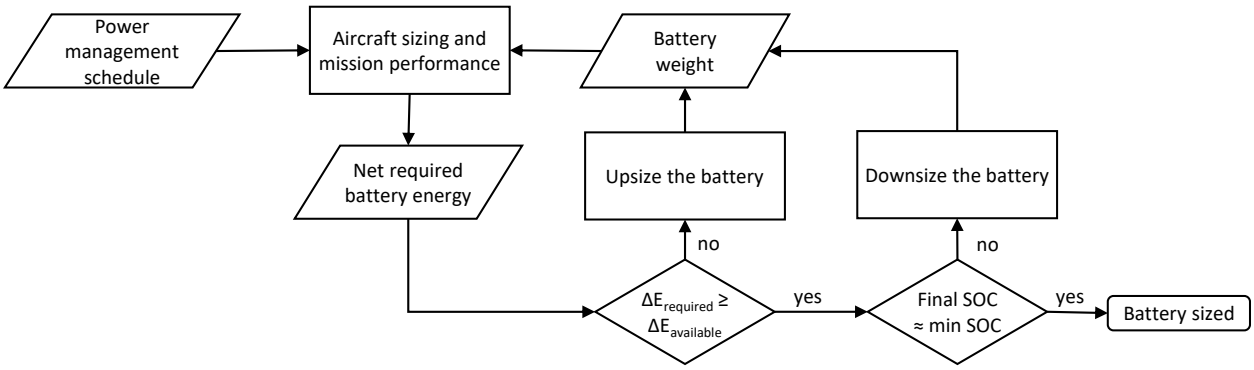

Fig. 10 Flowchart for the battery sizing logic.

V. Trade Studies and Mission Analysis Results

In order to be able to quantify any benefit or drawback, the baseline vehicle was run through the mission as a control. Figure 11 shows the mission history of the baseline vehicle for the mission profile given in Figure 4. The mission endurance was 18 hours and required approximately 3250 lbs of fuel. Because of its large wingspan, the vehicle also has a large lift to drag ratio of approximately 24 through most of the mission. A majority of the mission is spent in either the cruise segments or loiter segments however the peak power requirements are from the climb segment as the vehicle climbs to 35,000 ft in just under 40 minutes.

As mentioned previously, the vehicle maximum take off weight was to remain constant so a trade off was necessary to accommodate the additional weight of the generator, electric motor and, if applicable, the battery in the system. Such a trade off could be made between the battery and payload and/or endurance. This study investigates the feasibility of a hybrid/turboelectric architecture for the same mission performance of the baseline vehicle. Therefore, endurance could not be traded off. For the cases where the additional weight was not offset by the performance of the electrified propulsion system, maximum payload capacity was decreased. A similar study can be carried out by trading the endurance while keeping a fixed payload consistent with the baseline.

Four experiments were run to look at different battery utilization strategies and their impact on the vehicle's climb performance and payload weight trade off.

Case 1. Turboelectric: No battery

Case 2. Hybrid Turboelectric: Battery is sized for e-boost for the first climb segment. Battery is discharged during climb and charged during first cruise.

Case 3. Hybrid Turboelectric: Battery is sized for e-boost for the first climb segment. Battery is discharged during climb, charged during first cruise, and discharged again during second cruise.

Case 4. Hybrid Turboelectric: Similar to Case 2 but battery is sized according to more demanding segment between climb and cruise.

The first of these cases is a purely turboelectric architecture which includes a generator and motor, but removes the engine accessories which are no longer required with the addition of the electrical components. The next series of cases look at discharging the battery during the climb segment and then recharging the battery to full capacity during the subsequent cruise segment. A notional mission profile with these scenarios are given in Figure 12.

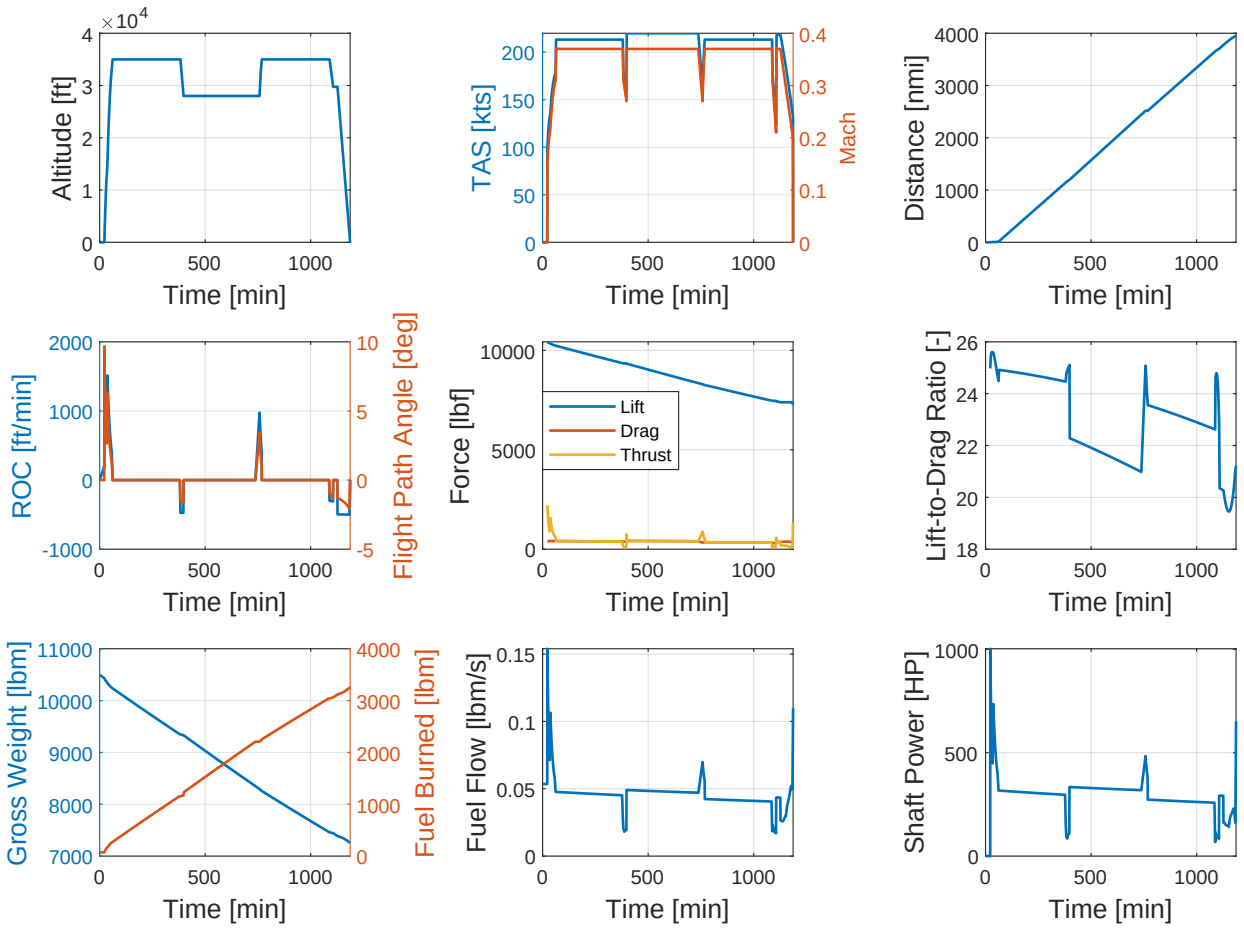

Fig. 11 Mission history of the baseline vehicle.

In Case 2, the battery is charged in flight either to maintain excess energy to provide a high peak load, or for a quick turn-around time. Figure 12a shows how this charging and discharging scenario is implemented during the mission with segments in red representing discharging the battery and segments in green charging the battery. The battery size is determined by the energy required and power split during the climb segment.

Cases 3 and 4 are similar to the previous ones in that the battery is discharged during climb and charged during the subsequent cruise, but the battery is then discharged again during the second cruise segment, as depicted in Figure 12b. Cases 3 and 4 are identical in terms of operational strategy. However, they use different sizing points for the battery. In Case 3, the battery size has been determined by the energy required and power split during the climb segment. In contrast, the battery in Case 4 is sized to the more demanding of the climb or the cruise segments.

For the hybrid cases (Cases 2, 3 and 4) a design of experiments was created to test different power management strategies for both the climb and second cruise segment and the power split was varied between 5% and 30% of the required power at the input of the electric motor. Results for the first three series of cases are shown below in Figures 13a, 13b, and 14.

The additional weight of the generator and motor is not offset by the weight removed from the engine accessories. As a result, the turboelectric case not only requires a bit more power to overcome this weight, but also suffers from losses in the generator and motor. This results in a fuel burn higher than for the baseline cases while also suffering a penalty in payload weight and time to climb.

Figure 13a clearly shows that Case 3 will require less fuel than Case 2 and that break even points are significantly different for the two cases. For Case 3, even below a battery split of 10% the fuel burn is still greater than the baseline. This is likely due to the fact that smaller battery splits do not provide enough excess power to overcome the losses in the generator and motor. These losses vary throughout the climb segment, but typically make up about an 8-10% loss in

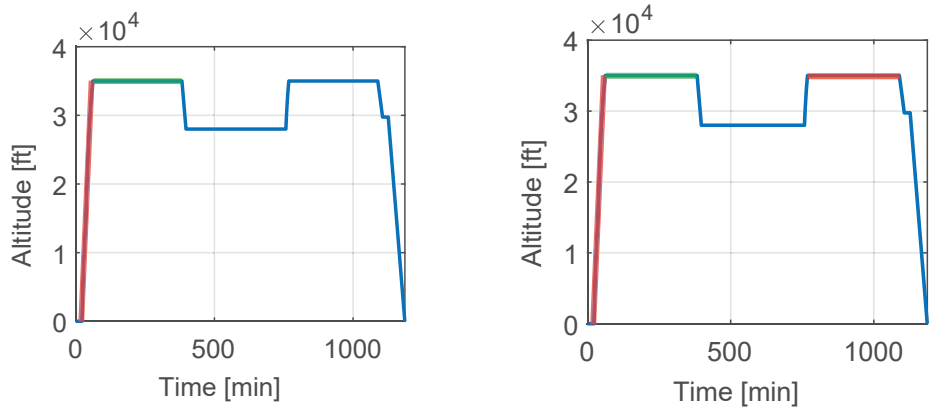

(a) **(b)**

Fig. 12 Battery charging and discharging logic during mission for (a) Case 2, and (b) Case 3. Red highlight represents discharging, green represents charging.

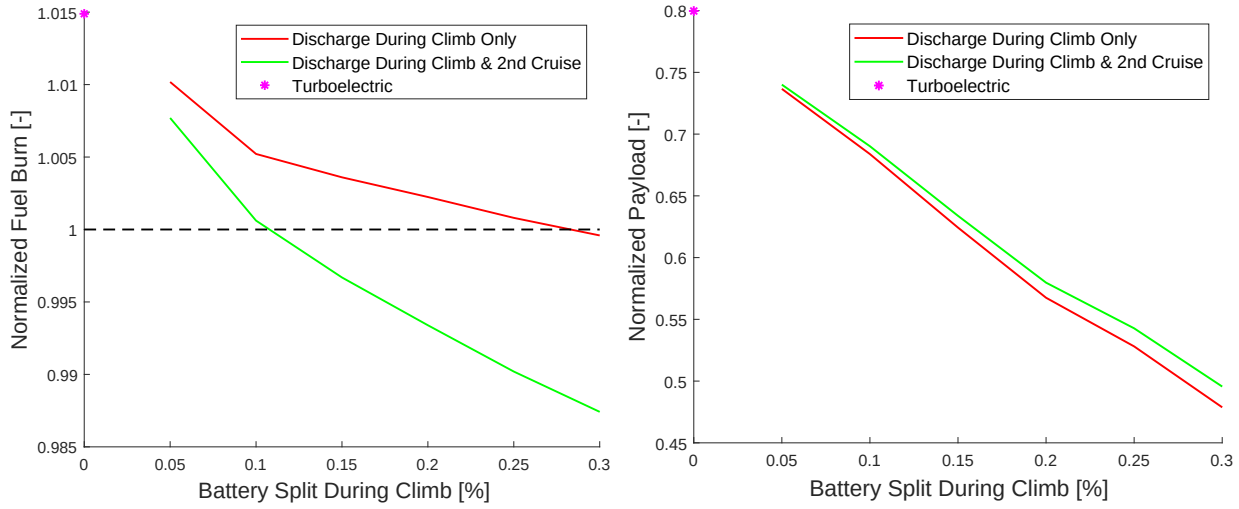

(a) Case 2 **(b) Case 3**

Fig. 13 (a) Normalized fuel burn and (b) normalized payload weight results for the turboelectric and hybrid turboelectric cases.

power. Above a 10% battery power split, a reduction in fuel burn is seen when the battery is discharged completely. When the battery must be recharged, fuel must be used to power the generator and pull additional power so an increase in fuel burn is expected, but still a break even point is reached at about a 30% split.

The reduction in fuel burn does not completely offset the battery weight as a larger battery is significantly heavier than the savings in fuel weight, but this is expected as fuel has a much higher energy density compared to batteries. Although a turboelectric architecture requires the most fuel and increases time to climb, it requires the lowest trade off of payload weight. As expected, larger batteries eat away at the payload more than smaller batteries despite some fuel savings. The major benefit of the addition of batteries is the time saved during the climb segment. This savings in time also corresponds to some amount of fuel savings as well because the engine is running for a shorter period of time. Time to climb is not affected by usage of the battery during the second cruise phase so the results for the cases of discharging the battery then or not are identical. Similar to the fuel burn results, time to climb only decreases below the baseline value at and above a 10% split in power for the same reasons as mentioned previously.

The results for the final series of cases regarding the battery sizing are shown below in Figure 15. The different

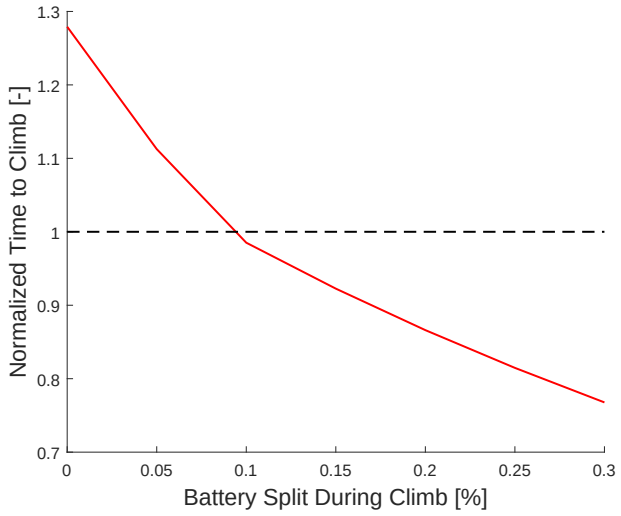

Fig. 14 Normalized time to climb for the first climb segment for turboelectric and hybrid electric UAV.

color lines represent different battery power split values during the second cruise segment while the black dotted line represents a battery split of 0% during the second cruise segment. At a battery split above 5% during the second cruise, the lines are all horizontal which indicates that the battery is being sized strictly for that cruise segment. For this mission, cruise segments are much longer than climb segments so for the same battery split, the cruise will require more energy and the results agree with this. Looking at a battery split of 5% during the cruise, however, shows that there is a change in the sizing point of the battery. For these cases, when the battery split during the climb increases above 20% the battery transitions from being sized for the cruise energy to being sized for the climb energy. For larger climb battery split values the sizing point could also change with higher cruise battery splits, however the battery size will increase drastically. Only so much payload and saved fuel weight can be traded for battery and electrical component weight so there is a cap on the allowable battery splits during each segment. With improved battery technology and and increase in specific energy these larger battery split scenarios could become feasible.

VI. Conclusion and Future Work

This paper presented the results of feasibility analysis and trade-off studies of electrification of a MALE UAV. Electrified propulsion systems considered included turboelectric and hybrid turboelectric architectures. A retrofit study was conducted where the critical mission and point performance requirements such as endurance and peak power were kept fixed. Payload was traded off with the additional weight and reduction in the powertrain efficiency due to the installation of the electrical components. For the hybrid architectures, different power management strategies were used to size the battery and identify the best usecase.

For the hybrid cases, hybridization of the first (and longest) climb segment decreased the minimum time to climb compared to the baseline and turboelectric cases. This improvement in the climb performance is primarily due to the e-boost provided by the battery as it generates additional excess power which was not available before due to the lapsing turboshaft engine. By spending this excess power on increasing the rate of climb, a shorter climb time was achieved. The shorter climb also provided fuel burn benefits above 30% power split at the cost of significantly increased battery weight.

Other scenarios were also played out where the battery is charged in flight and discharged again during the second cruise segment at varying hybridization levels. The hybridization of cruise and re-use of the battery after it was fully charged in flight provided further fuel burn savings above 10% power split. These savings bought back some payload, but the maximum payload capacity was still severely reduced.

Overall, the results were not surprising: the hybrid/turboelectric architectures were not able to offset the considerable weight addition and electrical losses under any of the feasible power management strategies for the same point performance and mission requirements of the baseline aircraft with a conventional propulsion system. This means that in order to make room for the new powertrain, maximum payload capacity must be reduced considerably.

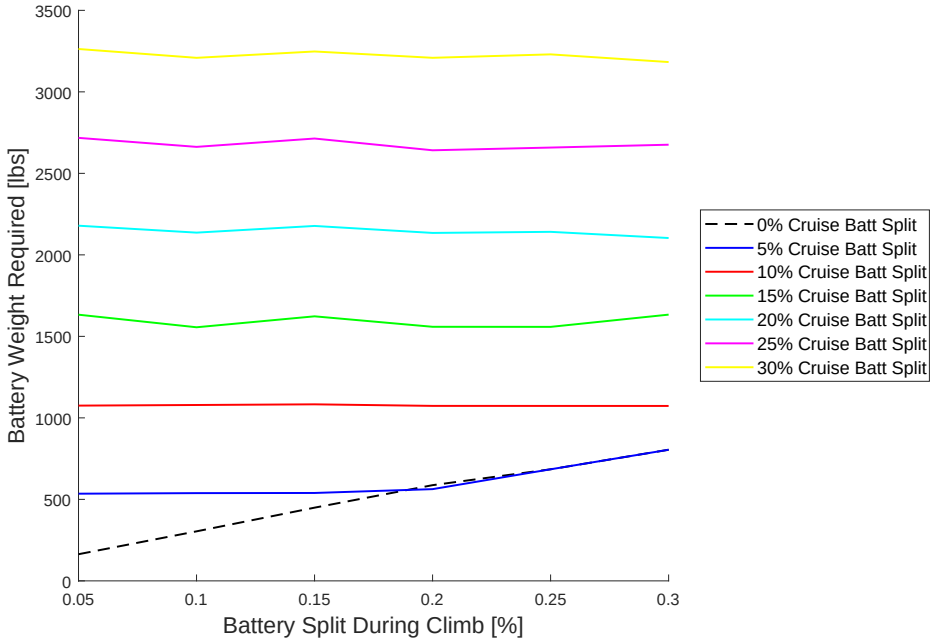

Fig. 15 Battery size variation for different power splits during the climb and second cruise segments.

Although electrification of the propulsion system comes with its cost, electric power can still be beneficial due to its ability to provide high peak powers faster than the turboshaft engine. This was observed in the improvement of the climb performance of the aircraft thus indicating that for missions that require more aggressive climb performance compared to the baseline mission, hybrid turboelectric propulsion can provide potential benefits. Net fuel burn savings were obtained when the battery was charged in flight and discharged again during a long cruise segment. These results are promising for the second phase of this research where the engine and battery power are going to drive multiple propellers distributed over the wings. Distributed propulsion systems are enabled by the turboelectric architecture by making use of the locational flexibility it brings and can provide aerodynamic benefits to the system. Together with the improved climb performance, fuel burn savings and increased aerodynamic efficiency, the additional weight and electrical losses associated with the hybrid/turboelectric power train could be offset under the right power management strategy.

In addition to the consideration of a distributed propulsion system, future work will include the usage of optimization techniques to find the optimum power split and battery size, as described by the lead author in Ref. [27]. This study assumed state-of-the-art technology levels for the electrified propulsion subsystems. Sensitivity studies will be performed to identify technology targets for the battery, motor and generator. Finally, this retrofit study will be extended to an aircraft sizing study where the weight of the electrified powertrain will impact the takeoff gross weight while the payload capacity will be kept frozen. Such a study would also benefit greatly from the consideration of volumetric limitations and structural implications.

Acknowledgments

The authors would like to acknowledge Ariel Tokarz for her contributions in the literature survey. The authors would also like to thank AFRL for providing funding and insight for this research.

References

[1] Miranda, D., "2020 NASA Technology Taxonomy," Tech. rep., 2020.

[2] Welstead, J., Felder, J., Guynn, M., Haller, B., Tong, M., Jones, S., Ordaz, I., Quinlan, J., and Mason, B., "Overview of the NASA STARC-ABL (rev. B) advanced concept," 2017.

[3] Kim, H. D., Felder, J. L., Tong, M. T., and Armstrong, M., "Revolutionary aeropropulsion concept for sustainable aviation: turboelectric distributed propulsion," 2013.

[4] Schiltgen, B. T., and Freeman, J., "ECO-150-300 design and performance: a tube-and-wing distributed electric propulsion airliner," *AIAA Scitech 2019 Forum*, 2019, p. 1808.

[5] Chau, K., and Wong, Y., "Overview of power management in hybrid electric vehicles," *Energy conversion and management*, Vol. 43, No. 15, 2002, pp. 1953–1968.

[6] Khajepour, A., Fallah, M. S., and Goodarzi, A., *Electric and hybrid vehicles: technologies, modeling and control-a mechatronic approach*, John Wiley & Sons, 2014.

[7] Litherland, B., Borer, N., and Geuther, S., "A Study on the Use of Solid-Oxide Fuel Cells for Increased Power Generation on Small Aircraft," *AIAA Aviation*, 2019.

[8] Finger, D. F., Braun, C., and Bil, C., "Comparative assessment of parallel-hybrid-electric propulsion systems for four different aircraft," *Journal of Aircraft*, 2020, pp. 1–11.

[9] Fioriti, M., Vaschetto, S., Corpino, S., and Premoli, G., "Design of hybrid electric heavy fuel MALE ISR UAV enabling technologies for military operations," *Aircraft Engineering and Aerospace Technology*, 2020.

[10] Cinar, G., Emeneth, M., and Mavris, D. N., "A Methodology for Sizing and Analysis of Electric Propulsion Subsystems for Unmanned Aerial Vehicles," *54th AIAA Aerospace Sciences Meeting*, 2016.

[11] Alex, D., "BAe Systems Mantis Unmanned Aircraft," , Mar 2016. URL https://www.militaryfactory.com/aircraft/detail.asp?aircraft_id=1028.

[12] Airbus, "European MALE RPAS," , 2019. URL https://www.airbus.com/newsroom/events/ila-2018/EuroMale.html.

[13] Aeronautical, G. A., "Predator B," , 2019. URL https://www.ga-asi.com/images/products/aircraft_systems/pdf/Predator_B021915.pdf.

[14] "Piaggio Aerospacespace - P.1HH HammerHead," , 2019. URL http://www.p1hh.piaggioaerospace.it/.

[15] Aurora, "Orion Medium-Altitude Long-Endurance Umanned Aircraft," , 2019. URL https://www.aurora.aero/wp-content/uploads/2015/10/Orion-Brochure_web_X3.pdf.

[16] "Heron TP (Eitan)," , Aug 2015. URL https://militaryedge.org/armaments/heron-tp-eitan/.

[17] "RQ-4 Global Hawk," , Oct 2014. URL https://www.af.mil/About-Us/Fact-Sheets/Display/Article/104516/rq-4-global-hawk/.

[18] Aerospace, B., "Bell V-247 Vigilant," , 2020. URL https://www.bellflight.com/products/bell-v-247.

[19] Aeronautics, "Dominator XP MALE UAS," , 2019. URL http://aeronautics-sys.com/home-page/page-systems/page-systems-dominator-xp-male-us/.

[20] Times, L. A., "Firebird spy plane at a glance," , May 2011. URL https://www.latimes.com/business/la-xpm-2011-may-09-la-fi-northrop-drone-box-20110509-story.html.

[21] Pendergast, S., "ADCOM Yabhon United 40 (Smart Eye 2) UAV," , Sep 2014. URL http://spendergast.blogspot.com/2014/09/adcom-yabhon-united-40-smart-eye-2-uav.html.

[22] Pike, J., "Chang Hong-5 (CH-5) combat and reconnaissance drone," , 2019. URL https://www.globalsecurity.org/military/world/china/ch-5.htm.

[23] "Military Factory," , 2019. URL https://www.militaryfactory.com/.

[24] "AT200 Cargo Unmanned Ariel Vehicle," , 2019. URL https://www.aerospace-technology.com/projects/at200-cargo-unmanned-aerial-vehicle/.

[25] Chiesa, S., Farfaglia, S., Fioriti, M., and Viola, N., "Design of all electric secondary power system for future advanced medium altitude long endurance unmanned aerial vehicles," *Proceedings of the Institution of Mechanical Engineers, Part G: Journal of Aerospace Engineering*, Vol. 226, 2011, pp. 1255–1270.

[26] DrawingDatabase, "General Atomics MQ-9 Reaper Blueprint," , 2019. URL https://drawingdatabase.com/mq-9-reaper/.

[27] Cinar, G., "A methodology for dynamic sizing of electric power generation and distribution architectures," Ph.D. thesis, Georgia Institute of Technology, 2018.

[28] Cinar, G., Garcia, E., and Mavris, D. N., "A framework for electrified propulsion architecture and operation analysis," *Aircraft Engineering and Aerospace Technology*, Vol. 92, No. 5, 2019, pp. 675–684.

[29] Anderson, J., *Aircraft Performance and Design*, WCB/McGraw-Hill, 2012, 2012.

[30] Brandt, S., *Introduction to Aeronautics: A Design Perspective*, American Institute of Aeronautics and Astronautics, Inc., 2015.

[31] Honeywell, "TPE331-10 TURBOPROP ENGINE," Brochure, 2016. URL https://aerospace.honeywell.com/content/dam/aero/en-us/documents/learn/products/engines/brochures/N61-1491-000-000-TPE331-10TurbopropEngine-bro.pdf.

[32] Hamilton, S., "Generalized Method of Propeller Performance Estimation 1961-1963," , 1963. URL https://open.bu.edu/handle/2144/10454.